Model-Free Predictive Current Control of DFIG Based on an Extended State Observer Under Unbalanced and Distorted Grid

Yongchang Zhang, *Senior Member, IEEE*, Tao Jiang, and Jian Jiao

***Abstract*—The traditional method of controlling a doubly fed induction generator based on a mathematical model has poor control performance when the motor parameters are inaccurate. To solve this problem, this article proposes a new model-free predictive current control (MFPCC) scheme. In the proposed method, an ultralocal model is used to replace the mathematical model of the motor, and an extended state observer (ESO) is used to estimate the value of the disturbance to improve the control performance. Since only the measured stator voltage and current values are required in the final control expression, the control system achieves good parameter robustness. In addition to superior control performance when the parameters are inaccurate, the proposed method also has good steady state and dynamic performance when the parameters are accurate. The proposed MFPCC scheme based on an ESO is extended to an unbalanced and distorted grid by modifying the stator current reference. The presented experimental results confirm the effectiveness of the proposed method.**

***Index Terms*—Predictive control, doubly fed induction generator (DFIG), model-free, observer, nonideal grid.**

I. Introduction

With the continuous development of the economy, industrial applications based on new and clean energy sources have become increasingly valuable. As a renewable energy source, wind power is developing rapidly. Due to its outstanding advantages, including power decoupling control, maximum wind power capture ability, and relatively low cost, the doubly fed induction generator (DFIG) is employed on a large scale in wind power generation. Thus, control methods for the DFIG have been a research focus in both academic and industrial communities. Recently, research on brushless doubly fed induction machines (BDFMs) has received an increasing amount of attention [1]. Compared with those of the DFIG, the power winding and control winding of the BDFM are indirectly coupled through the rotor winding, eliminating the slip ring or the brush; its structure is more complicated and control is more difficult, but its basic principle is similar to that of the DFIG.

As a control method for a DFIG, vector control [2] can obtain good steady-state performance, but it is necessary to design appropriate proportional-integral (PI) parameters, and the dynamic performance is not ideal. Direct power control (DPC) [3] is simple, and the dynamic performance is good; however, this approach produces a high-power ripple at steady state. The improved method of DPC based on space vector modulation (DPC-SVM) [4] can achieve deadbeat control over the power, but the method is more complicated. Model predictive control (MPC) [5] can achieve both steady state and dynamic performance simultaneously, but requires many motor parameters and involves considerable calculation.

In practical applications, the system is affected by internal and external disturbances. Assuming that the sensor measurement is accurate, the internal disturbance of the doubly fed motor is mainly due to a parameter change or a parameter mismatch. For example, the stator/rotor resistance may change due to temperature variation, and the mutual inductance of a DFIG may become saturated due to a large conducting current under a sudden grid change. External disturbances mainly include changes in the grid voltage, including imbalance, distortion, and frequency changes. When disturbances occur, the performance of conventional control methods may deteriorate significantly if the disturbance is not taken into consideration.

For internal disturbances, to improve the parameter robustness of a control method, researchers have proposed a variety of solutions, and these solutions can be classified into three categories.

The methods in the first category solve the problem of parameter robustness based on online parameter identification. For example, in [6], a recursive least squares method is employed to estimate the parameters of a DFIG online when the motor parameters change.

The robust control methods in the second category are based on a disturbance observer or an extended state observer (ESO), and one of the most popular methods is active disturbance rejection control (ADRC). In [7], a disturbance observer was added to the control loop of a continuous time prediction control method. With this method, when the motor parameters change or an external disturbance occurs, the motor can still maintain good control performance. In [8], MPC based on an ESO is applied to a permanent magnet synchronous motor (PMSM).

Manuscript received August 15, 2019; revised December 10, 2019; accepted January 9, 2020. Date of publication January 15, 2020; date of current version April 22, 2020. This work was supported in part by the National Natural Science Foundation of China under Grant 51577003. Recommended for publication by Associate Editor W. Cao. *(Corresponding author: Yongchang Zhang.)*

The authors are with the Inverter Technologies Engineering Research Center of Beijing, North China University of Technology, Beijing 100144, China (e-mail: yozhang@ieee.org; jiangtao1130@qq.com; 79157937@qq.com).

Color versions of one or more of the figures in this article are available online at https://ieeexplore.ieee.org.

Digital Object Identifier 10.1109/TPEL.2020.2967172

However, it presents variable switching frequency, and only simulation results are presented. For a standalone DFIG, Guo *et al.* [9] proposed direct voltage control based on nonsingular terminal sliding mode control and an improved ESO, which has good control performance, but more parameters need to be designed. In [10] and [11], ADRC is applied to a DFIG to suppress the disturbance of motor parameters. However, as the rotor current reference value is calculated using the mutual inductance, it has limited ability to suppress the influence of mutual inductance changes. Furthermore, it considers only ideal grid voltage conditions.

Recently, model-free control schemes have been proposed in the literature to solve the problem of parameter robustness. In [12], the researchers proposed a model-free control scheme based on a current difference for PMSMs. However, this method requires a high sampling frequency to achieve satisfactory performance. When two or more adjacent control periods apply the same voltage vector, the update of the current difference is affected, which results in a poor control performance. An ultralocal model combined with proportional-integral-derivative control technology was proposed in [13]. This method achieves good control performance for both linear and nonlinear systems and has good parameter robustness. Recently, the application of the model-free control introduced in [13] was extended to power electronic drives, as shown in [14] for a PMSM drive.

For external disturbances, the research works in[15]–[20] proposed control methods for suppressing the current harmonics under unbalanced and/or distorted grid conditions. In [15], a repetitive controller is added to the current loop to eliminate $6n \pm 1$-order harmonics in the stator current. Because the motor parameters are used in the calculation of the rotor current reference value, its control performance will be affected by changes in the motor parameters. In [16], a nonlinear backstepping algorithm is proposed to suppress current harmonics. In [17], the conventional power theory is replaced by extended power theory to achieve sinusoidal stator currents, even under an unbalanced network. However, these methods are still parameter-dependent. Sliding-mode DPC (SM-DPC) [18], [19] and H-infinity control [20] have also been proposed in the literature to eliminate the effects of parameter perturbations and external voltage perturbations. However, the control complexity is also increased, and much tuning work is required.

To the best of the authors' knowledge, the power control of a DFIG based on model-free control has not yet been reported in the literature. For the first time, this article introduces the concept of model-free control to the power control of a DFIG to solve the problem of machine parameter dependence. The rotor reference voltage vector is subsequently calculated based on the principle of deadbeat current control and then synthesized by SVM. Furthermore, model-free control under an unbalanced and distorted network is also investigated to achieve sinusoidal stator currents while satisfying the requirements of power control.

The structure of this article is as follows. Section I introduces the background of the research. Section II mainly introduces the mathematical model of the doubly fed machine. Section III introduces the principle of the proposed method in detail and proves its validity in theory. Section IV presents the control method under an unbalanced and distorted grid. Section V presents experimental results that verify the effectiveness of the proposed method. Section VI presents the summary of the article.

II. Dynamic Equations of a DFIG

Because the output voltage of a two-level inverter is directly applied to the rotor side of a DFIG, the mathematical model of a DFIG in the rotor reference frame is concise and practical and can be expressed as [21]

$$\boldsymbol{u}_s = R_s \boldsymbol{i}_s + \frac{d\boldsymbol{\psi}_s}{dt} + j\omega_r \boldsymbol{\psi}_s \tag{1}$$

$$\boldsymbol{u}_r = R_r \boldsymbol{i}_r + \frac{d\boldsymbol{\psi}_r}{dt} \tag{2}$$

$$\boldsymbol{\psi}_s = L_s \boldsymbol{i}_s + L_m \boldsymbol{i}_r \tag{3}$$

$$\boldsymbol{\psi}_r = L_m \boldsymbol{i}_s + L_r \boldsymbol{i}_r \tag{4}$$

where $\boldsymbol{u}_s$, $\boldsymbol{u}_r$, $\boldsymbol{i}_s$, $\boldsymbol{i}_r$, $\boldsymbol{\psi}_s$, and $\boldsymbol{\psi}_r$ are the stator voltage vector, rotor voltage vector, stator current vector, rotor current vector, stator flux vector, and rotor flux vector, respectively; R_s, R_r, L_s, L_r, and L_m are the stator resistance, rotor resistance, stator inductance, rotor inductance, and mutual inductance, respectively, ω_r is the electrical rotor speed, and all variables have been converted to the stator side.

According to the principle of DPC-SVM [17], the rotor reference voltage can be obtained as

$$\begin{aligned}\boldsymbol{u}_r^{\text{ref}} = {} & \frac{2(\boldsymbol{S} - \boldsymbol{S}^{\text{ref}})^*}{3\lambda L_m T_{sc} \boldsymbol{u}_s^*} - \frac{\lambda L_r R_s + j\omega_{sl}}{\lambda L_m} \boldsymbol{i}_s \\ & - \frac{jL_r\omega_r}{L_m} \boldsymbol{\psi}_s + \frac{L_r}{L_m} \boldsymbol{u}_s + R_r \boldsymbol{i}_r \end{aligned} \tag{5}$$

$$\omega_{sl} = \omega_s - \omega_r \tag{6}$$

$$\boldsymbol{S} = P + jQ = \frac{3}{2} \boldsymbol{i}_s^* \boldsymbol{u}_s \tag{7}$$

where $\lambda = 1/(L_s L_r - L_m^2)$, $\boldsymbol{S}$, P, and Q are the stator-side complex power, active power, and reactive power, respectively, j is the imaginary unit, ω_s is the stator-side voltage angular frequency, T_{sc} is the sampling period, and the superscripts $*$ and ref indicate conjugate complex numbers and reference values, respectively.

The parameter dependence of (5) is analyzed as follows. Under normal conditions, the mutual inductance is much bigger than the leakage inductance of the stator and rotor, which means $L_m \gg L_{ls}$, $L_m \gg L_{lr}$, and $L_m \approx L_r \approx L_s$. Hence, the expression of λL_m can be approximated as

$$\begin{aligned}\lambda L_m = \frac{L_m}{L_s L_r - L_m^2} &= \frac{L_m}{(L_{ls} + L_m)(L_{lr} + L_m) - L_m^2} \\ &\approx \frac{1}{L_{ls} + L_{lr}} \end{aligned} \tag{8}$$

and (5) can be rewritten as

$$\boldsymbol{u}_r^{\text{ref}} \approx \frac{2(\boldsymbol{S} - \boldsymbol{S}^{\text{ref}})^*}{3T_{sc}\boldsymbol{u}_s^*}(L_{ls} + L_{lr}) - j\omega_{sl}(L_{ls} + L_{lr})\boldsymbol{i}_s + \boldsymbol{u}_s$$

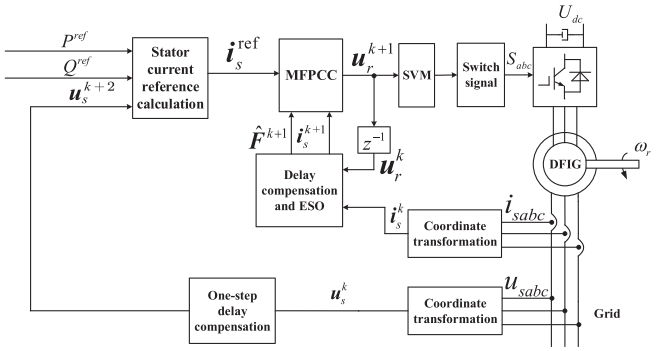

Fig. 1. Control diagram of the proposed method.

$$- R_s \boldsymbol{i}_s - j\omega_r L_m(\boldsymbol{i}_s + \boldsymbol{i}_r) + R_r \boldsymbol{i}_r. \tag{9}$$

It can be seen from (9) that in DPC-SVM, changes in the stator resistance, rotor resistance, and mutual inductance will cause changes in the rotor voltage, but the influence of the mutual inductance is greater because it is multiplied by the rotor speed. In this article, we compare the control performance of the proposed method with that of DPC-SVM under the conditions of a change in the mutual inductance parameters. The experimental results are shown in Section V.

III. Principle of the Proposed Method

To improve the control performance under the condition of a parameter variation, this article applies an ultralocal model of a DFIG based on an ESO to PCC. A block diagram of the control scheme is shown in Fig. 1. The scheme mainly consists of the following parts: one-step delay compensation, reference calculation, MFPCC, and the ESO. The details of the proposed method are explained in the following parts.

A. Stator Current Reference Calculation

Due to the one-step delay in the digital implementation [21], the rotor voltage vector obtained at time k is not applied until the next time $k+1$. To eliminate this delay, the stator side current value at time $k+2$ is calculated as the stator current reference value by the stator-side reference complex power, as shown below

$$\boldsymbol{i}_s^{\text{ref}} = \frac{2}{3}\left(\frac{\boldsymbol{S}^{\text{ref}}}{\boldsymbol{u}_s^{k+2}}\right)^* \tag{10}$$

$$\boldsymbol{u}_s^{k+2} = \boldsymbol{u}_s^k\left(1 + j2\left(\omega_s - \omega_r\right)T_{sc}\right) \tag{11}$$

where the stator is directly connected to an ideal grid, and $\boldsymbol{u}_s$ is equal to the grid voltage.

B. Principle of MFPCC Based on an Ultralocal Model

For a system, according to [13], [22], a change in its input and output can be approximated as a finite-dimensional differential equation, specifically expressed as

$$E\left(t, y, y^{(1)}, \ldots, y^{(n)}, u, u^{(1)}, \ldots, u^{(m)}\right) = 0 \tag{12}$$

where y and u are the system output and input, respectively, E is an unknown but derivable function at most points, and the superscripts (n) and (m) are system orders. An ultralocal model can be used to describe the entire control system

$$y^{(n)} = \alpha u + F \tag{13}$$

where α is the coefficient of the input variable and its role is to adjust the order of magnitude of the input quantity u to the order of magnitude of F. It should be noted that α is a numerical value obtained through experience, and the error and is not precisely defined in advance. F is a variable containing the known structure, unknowns, and some disturbances of the system. The ultralocal model, which is updated in real time, can be seen as an approximation of the system model, where F must be updated in real time. F can be calculated from the estimates of α, u, and $y^{(n)}$.

According to the mathematical equations of the DFIG (1)–(4), the differential expression of the stator current can be calculated as follows:

$$\frac{d\boldsymbol{i}_s}{dt} = -\frac{\boldsymbol{u}_r}{\sigma L_m} + \left(-\frac{R_s L_r}{\sigma L_m^2}\boldsymbol{i}_s + \frac{R_r}{\sigma L_m}\boldsymbol{i}_r + \frac{L_r}{\sigma L_m^2}\boldsymbol{u}_s - \frac{j\omega_r L_r}{\sigma L_m^2}\boldsymbol{\psi}_s\right) \tag{14}$$

where $\sigma = \frac{L_s L_r - L_m^2}{L_m^2}$.

Equation (14) can be used as an expression for PCC. Combining (13) with (14), the MFPCC expression based on the ultralocal model of the DFIG is as follows:

$$\frac{d\boldsymbol{i}_s}{dt} = \alpha \boldsymbol{u}_r + \boldsymbol{F}. \tag{15}$$

Comparing (14) and (15), the correspondence between PCC and MFPCC can be obtained as

$$\begin{cases} \alpha = -\dfrac{L_m}{L_s L_r - L_m^2} \\ \boldsymbol{F} = -\dfrac{R_s L_r}{\sigma L_m^2}\boldsymbol{i}_s + \dfrac{R_r}{\sigma L_m}\boldsymbol{i}_r + \dfrac{L_r}{\sigma L_m^2}\boldsymbol{u}_s - \dfrac{j\omega_r L_r}{\sigma L_m^2}\boldsymbol{\psi}_s. \end{cases} \tag{16}$$

When the parameters change, the values of α and $\boldsymbol{F}$ become inaccurate, resulting in poor control performance. However, in MFPCC, although α is a predesigned constant and may not be an accurate value even when the parameters are accurate, it is possible to maintain good control performance by adjusting $\boldsymbol{F}$. For example, assume that α differs from the actual value, which can be expressed as

$$\alpha_1 = \alpha^{\text{ref}} + e \tag{17}$$

where α_1 is the control parameter used in controller, α^{ref} is the actual value of the system, and there is an error e between them. Because the total disturbance of the system can be replaced by $\boldsymbol{F}$, including unknown and known parts, it is reasonable to treat $e\boldsymbol{u}_r$ as part of the total disturbance. Then, (15) can be rewritten as

$$\frac{d\boldsymbol{i}_s}{dt} = \alpha_1 \boldsymbol{u}_r + \boldsymbol{F} = \alpha^{\text{ref}}\boldsymbol{u}_r + \underbrace{e\boldsymbol{u}_r + \boldsymbol{F}}_{\boldsymbol{F}^{\text{new}}} \tag{18}$$

where $\boldsymbol{F}^{\text{new}}$ is the new total disturbance of the system. Therefore, a method for obtaining the total disturbance of the system is crucial.

The works in [13] and [23] proposed a calculation method for the system variable $\boldsymbol{F}$, which uses the input and output variables of the system to estimate the variable $\hat{\boldsymbol{F}}$ and then uses this estimate to replace $\boldsymbol{F}$ in (13).

According to (15), by using the differential algebra method mentioned in the literature [24], it can be found that

$$\hat{\boldsymbol{F}} = -\frac{6}{L^3}\int_{t-L}^{t}\left(\left(L-2\sigma\right)\boldsymbol{i}_s(\sigma)+\alpha\sigma\left(L-\sigma\right)\boldsymbol{u}_r(\sigma)\right)d\sigma \tag{19}$$

where $L = n_F T_{sc}$, and n_F is the number of control periods in the integral step L. Using the gradient integral method to solve (19), the estimated value $\hat{\boldsymbol{F}}$ at time k is

$$\hat{\boldsymbol{F}} = -\frac{3}{n_F^3 T_{sc}}\sum_{k=1}^{n_F}\left(\boldsymbol{F}_1+\boldsymbol{F}_2\right) \tag{20}$$

where

$$\begin{cases}\boldsymbol{F}_1 &= \left(n_F-2\left(k-1\right)\right)\boldsymbol{i}_s(k-1)+\left(n_F-2k\right)\boldsymbol{i}_s(k)\\ \boldsymbol{F}_2 &= \alpha\left(k-1\right)T_{sc}\left(n_F-\left(k-1\right)\right)\boldsymbol{u}_r(k-1)\\ &\quad +\alpha k T_{sc}\left(n_F-k\right)\boldsymbol{u}_r(k).\end{cases} \tag{21}$$

When the system has a sudden load, such as a step change in the power reference value, more past information is used in the differential algebra method due to the existence of n_F, which may cause a slow dynamic response. To compensate for this shortcoming, this article uses an ESO to estimate this value.

C. Extended State Observer

The ESO expands the total disturbance (including the uncertain system variables and external disturbances) into a new one and feeds the total disturbance back to the controlled system so that control method of the system observes the nonlinear part of the model and the unknown external disturbance [25]. When using a nonlinear error function in the ESO, although a better control effect can be obtained, the computational complexity of the system is increased, and more parameters must be set. Thus, a linear ESO is used to replace the nonlinear error function with a linear error function. For a first-order single-input single-output system, it can be expressed as [26]

$$\begin{cases}\boldsymbol{e}_{rr} = \boldsymbol{z}_1 - \boldsymbol{y}\\ \dot{\boldsymbol{z}}_1 = \boldsymbol{z}_2 + \alpha\boldsymbol{u} - \beta_1\boldsymbol{e}_{rr}\\ \dot{\boldsymbol{z}}_2 = -\beta_2\boldsymbol{e}_{rr}\end{cases} \tag{22}$$

where $\boldsymbol{u}$ and $\boldsymbol{y}$ are the input and output of the observer, respectively, $\boldsymbol{z}_1$ and $\boldsymbol{z}_2$ are two state variables that need to be observed, β_1 and β_2 are observer parameters that must be set, and the superscript $\cdot$ indicates a differentiation of variables.

By combining (15) and (22) and considering the first-order Euler dispersion, an ultralocal model of the DFIG based on an ESO can be obtained

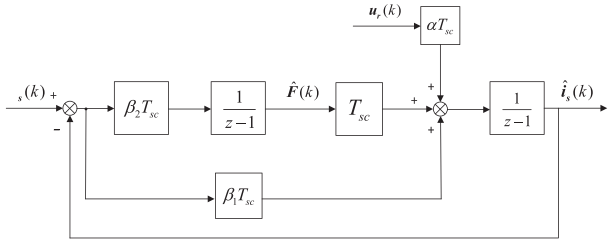

Fig. 2. Structural diagram of the ESO in the z-domain.

$$\begin{cases}\boldsymbol{e}_{rr}(k) = \hat{\boldsymbol{i}}_s(k) - \boldsymbol{i}_s(k)\\ \hat{\boldsymbol{i}}_s(k+1) = \hat{\boldsymbol{i}}_s(k) + T_{sc}\left(\hat{\boldsymbol{F}}(k)+\alpha\boldsymbol{u}_r(k)\right)\\ \qquad\qquad -\beta_1 T_{\text{sc}}\boldsymbol{e}_{rr}(k)\\ \hat{\boldsymbol{F}}(k+1) = \hat{\boldsymbol{F}}(k) - \beta_2 T_{sc}\boldsymbol{e}_{rr}(k)\end{cases} \tag{23}$$

where the superscript $\wedge$ indicates an estimated value of the variable.

According to (23), by taking the current measurement value as the input, the current estimation value as the output, and the voltage as the disturbance term, a structural diagram of the ESO in the z-domain can be obtained, as shown in Fig. 2. The closed-loop transfer function of the ESO of the DFIG is

$$G_c(z) = \frac{\beta_1 T_{sc} z - \beta_1 T_{sc} + \beta_2 T_{sc}^2}{\left(z-1\right)^2 + \beta_1 T_{sc} z - \beta_1 T_{sc} + \beta_2 T_{sc}^2}. \tag{24}$$

Let β_{11} denote $\beta_1 T_{sc}$ and β_{22} denote $\beta_2 T_{sc}$; then, the closed-loop characteristic equation of the system is

$$\lambda^2 + (\beta_{11}-2)\lambda + 1 - \beta_{11} + \beta_{22}T_{sc} = 0. \tag{25}$$

β_{11} and β_{22} will affect the closed-loop pole position of the system, thus affecting the final control performance of the system. When the entire root of the characteristic equation of the discrete system is distributed within the unit circle of the z-domain, the system is stable. After parameterization, the poles of the characteristic equation can be placed at the same position, which simplifies the design of the ESO [27]. Therefore, (25) can be rewritten as

$$(\lambda-\beta)^2 = 0 \tag{26}$$

where β is a common pole, also known as the discrete estimator bandwidth, which is the only tuning parameter for the ESO. Comparing (25) and (26), it can be obtained that

$$\begin{cases}\beta_{11} = 2\left(1-\beta\right)\\ \beta_{22} = \dfrac{\beta_{11}^2}{4T_{sc}}.\end{cases} \tag{27}$$

By the first-order forward difference method, the conversion relationship between the z-domain and the s-domain is

$$\frac{z-1}{T_{sc}} = s. \tag{28}$$

Thus, β corresponds to the bandwidth ω_0 in the continuous s-domain in [26], and the relationship is

$$\beta = 1 - \omega_0 T_{sc}. \tag{29}$$

According to [28], when ω_0 is small, the tracking performance of the observer is poor, and when ω_0 is large, the noise sensitivity will increase. Thus, a proper observer bandwidth should be selected as a compromise between the tracking performance and noise sensitivity. In this article, β is chosen as 0.75. According to (27), the corresponding values of β_{11} and β_{22} are 0.5 and 625, respectively.

After designing the parameters of the observer, taking into account the one-step delay, the final required rotor voltage can be obtained as

$$\boldsymbol{u}_r^{k+1} = \frac{(\boldsymbol{i}_s^{\text{ref}} - \boldsymbol{i}_s^{k+1})}{\alpha T_{sc}} - \frac{1}{\alpha}\hat{\boldsymbol{F}}^{k+1} \tag{30}$$

where, according to (23), $\boldsymbol{i}_s^{k+1}$ can also be obtained by the ESO

$$\boldsymbol{i}_s^{k+1} = \boldsymbol{i}_s^k + T_{sc}(\alpha \boldsymbol{u}_r^k + \hat{\boldsymbol{F}}^k). \tag{31}$$

It should be noted that the proposed method does not need to measure the rotor voltage value. The predicted rotor voltage value $\boldsymbol{u}_r^{k+1}$ will be stored in the memory and updated at all times. The rotor voltage value at the current time $\boldsymbol{u}_r^k$ can be obtained directly from the memory. Finally, the reference value $\boldsymbol{u}_r^{k+1}$ will be applied to the rotor side to control the entire DFIG system by SVM.

It can be seen from (30) and (31) that the required rotor voltage does not need any motor parameters; thus, the entire control system has good parameter robustness. The following experiments verify the effectiveness of the proposed method.

IV. Control Method Under an Unbalanced and Distorted Grid

In wind power systems, wind turbines are generally located in remote locations. Such weak grid systems may generate higher harmonic voltages at the wind turbine terminals. Harmonics in the grid voltage will affect the grid current, dc-bus voltage, stator current, rotor current, power, fan torque, and so on. Therefore, to maintain the stability of the wind power transmission system based on the DFIG, it is necessary to study the control algorithm under unbalanced and distorted grid conditions.

Because the three-phase system considered in this analysis assumes a three-wire connection system, the zero sequence component, and the third harmonic of the grid voltage can be ignored. To ensure the generality of the proposed method, this article considers the case of one-phase voltage dip and the fifth and seventh harmonics in the three-phase stator voltages. Therefore, the grid voltage contains positive, negative, and harmonic components

$$\begin{aligned}\boldsymbol{u}_g &= \boldsymbol{u}_g^+ + \boldsymbol{u}_g^- + \boldsymbol{u}_g^{5+} + \boldsymbol{u}_g^{5-} + \boldsymbol{u}_g^{7+} + \boldsymbol{u}_g^{7-} \\ &= \boldsymbol{u}_g^+ + \boldsymbol{u}_g^{\text{else}}\end{aligned} \tag{32}$$

where $\boldsymbol{u}_g^+$ is the fundamental voltage, and $\boldsymbol{u}_g^{\text{else}}$ is the sum of other negative sequences and each harmonic voltage. By using the MFPCC based on an ESO, active and reactive power are controlled by the stator current. Thus, according to (32), (10) can be rewritten as

$$\boldsymbol{i}_s^{\text{ref}} = \frac{2}{3}\left(\frac{\boldsymbol{S}^{\text{ref}}}{\boldsymbol{u}_g^+ + \boldsymbol{u}_g^{\text{else}}}\right)^*. \tag{33}$$

It can be seen from (33) that if the DFIG is still controlled to produce constant active and reactive power when the grid is unbalanced and distorted, then the stator current will also present positive, negative, and harmonic components [29]. To obtain sinusoidal and balanced stator currents under an unbalanced and distorted grid, the stator current reference should contain only the positive sequence component, as shown in (34). The key is the method by which the fundamental component of the grid voltage is extracted. This article uses the cascaded delayed signal cancellation [30] method to extract the fundamental component of the stator voltages and, then, calculates the stator current references. In this way, the proposed MFPCC method is still applicable to unbalanced and distorted grids. This claim will be verified by the experimental results in Section V

$$\boldsymbol{i}_s^{\text{ref}} = \frac{2}{3}\left(\frac{\boldsymbol{S}^{\text{ref}}}{\boldsymbol{u}_g^+}\right)^*. \tag{34}$$

TABLE I
System and Control Parameters

System parameter	Symbol	Value
Grid phase voltage	U_N	150 V
DC-bus voltage	U_{dc}	100 V
Rated power	P_N	1.5 kW
Rated frequency	f_N	50 Hz
Number of pole pairs	N_p	3
Stator resistance	R_s	4.57 Ω
Rotor resistance	R_r	3.228 Ω
Mutual inductance	L_m	214.57 mH
Stator inductance	L_s	225.40 mH
Rotor inductance	L_r	225.40 mH
Turn ratio	k	3.36
Sampling period	T_{sc}	100 μs

V. Experimental Results

To confirm the effectiveness of the proposed method, experimental tests are carried out on the DFIG system. The dSPACE is used as the controller, and peripheral hardware circuits and other parts, such as a two-level inverter, grid simulator, and bidirectional dc power supply, are used to verify the proposed method in the laboratory, as shown in Fig. 3. The system and control parameters used in the experimental tests are listed in Table I. Unless indicated, the initial rotor speed is 700 r/min. The parameters of the ultralocal model and ESO are as follows:

$$\begin{cases}\alpha = -40 \\ \beta_{11} = 0.5 \\ \beta_{22} = 625.\end{cases}$$

A. Responses Under Ideal Grids

Fig. 4 shows the experimental steady-state results of the proposed method. The active power reference value is −1000 W,

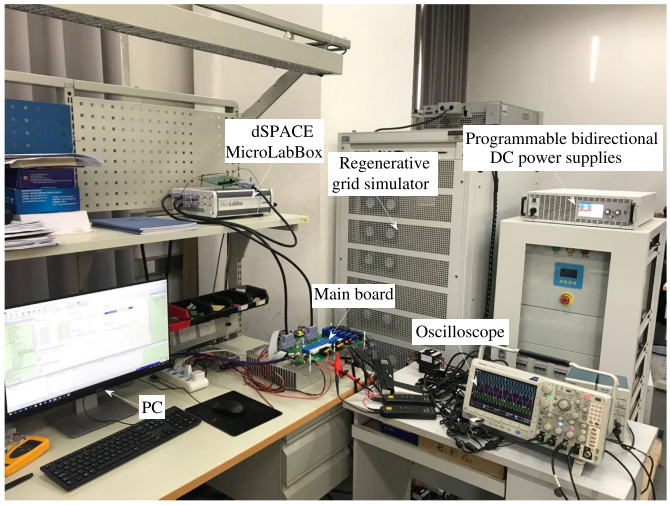

(a)

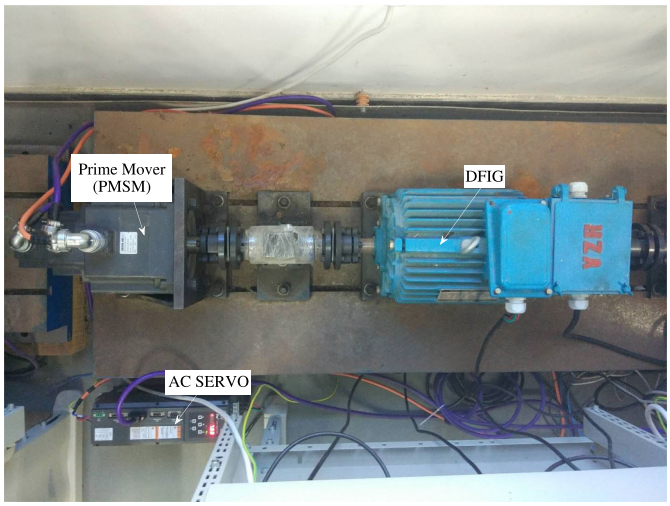

(b)

Fig. 3. Experimental platform for the DFIG system. (a) Control and main circuits. (b) DFIG and prime mover.

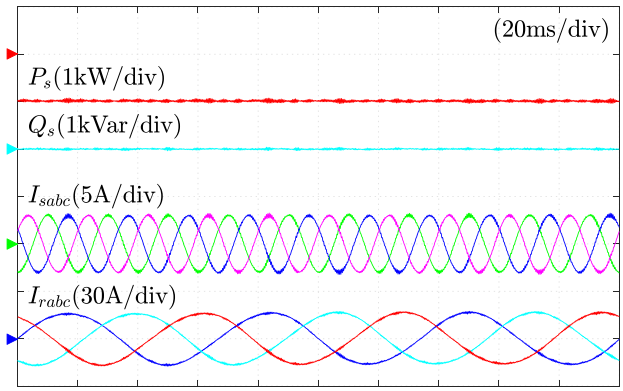

(a)

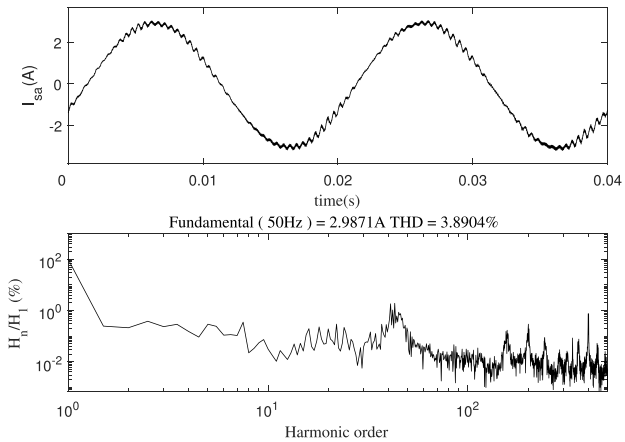

(b)

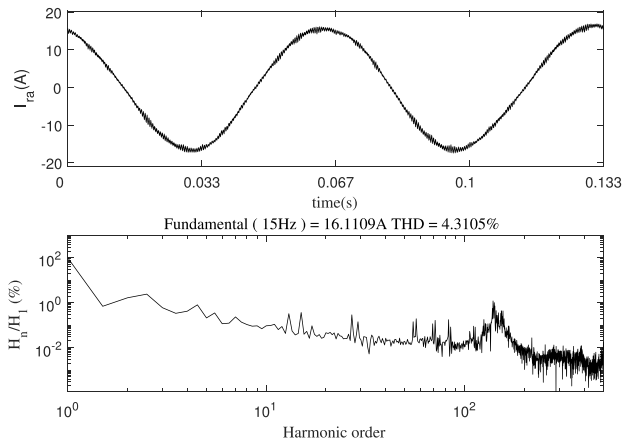

(c)

Fig. 4. Steady-state experimental results of MFPCC based on an ESO. (a) Response of active/reactive powers and three-phase stator/rotor currents. (b) Stator current THD. (c) Rotor current THD.

and the reactive power reference value is 0 Var. The control performance of the method is good at steady state. Fig. 4(b) and (c) shows the THD analysis of the current; the stator current THD is 3.89%, and the rotor current THD is 4.31%.

Figs. 5 and 6 show the dynamic experimental results of the proposed MFPCC using differential algebra and ESO. In Fig. 5, the reference active power steps from 0 to −1000 W at 0.1 s. It can be clearly seen that the MFPCC based on an ESO has a faster response than that based on differential algebra and has no overshoot. In Fig. 6, the rotor speed changes from 900 to 1100 r/min, where the reference active power is −750 W. The method based on an ESO can pass the synchronous speed more smoothly, and there are fewer rotor current harmonics and power ripples. Thus, using an ESO to estimate the total disturbance is more accurate in the dynamic response.

Fig. 7 shows the experimental results of the three methods for a change in the mutual inductance parameters, where the last channel k is the ratio between the inductance value used in the controller and the actual value. The variation range of the mutual inductance parameter is 50% and 150% of the rated value. The active reference value is always −1000 W. In Fig. 7(a), because DPC-SVM uses more motor parameters, there are more ripples and stator current harmonics with a change in

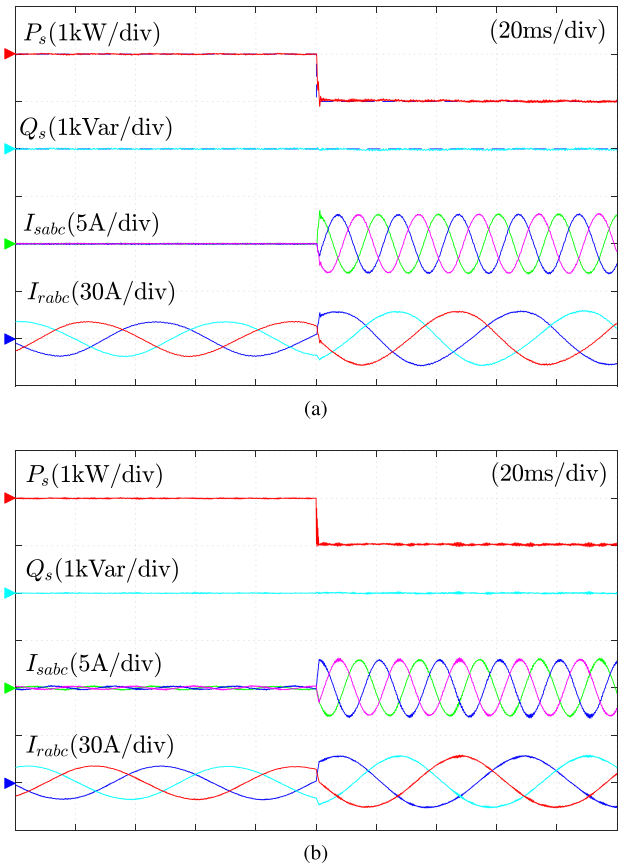

Fig. 5. Dynamic responses to stepped changes in the active power reference. (a) MFPCC based on differential algebra. (b) MFPCC based on an ESO.

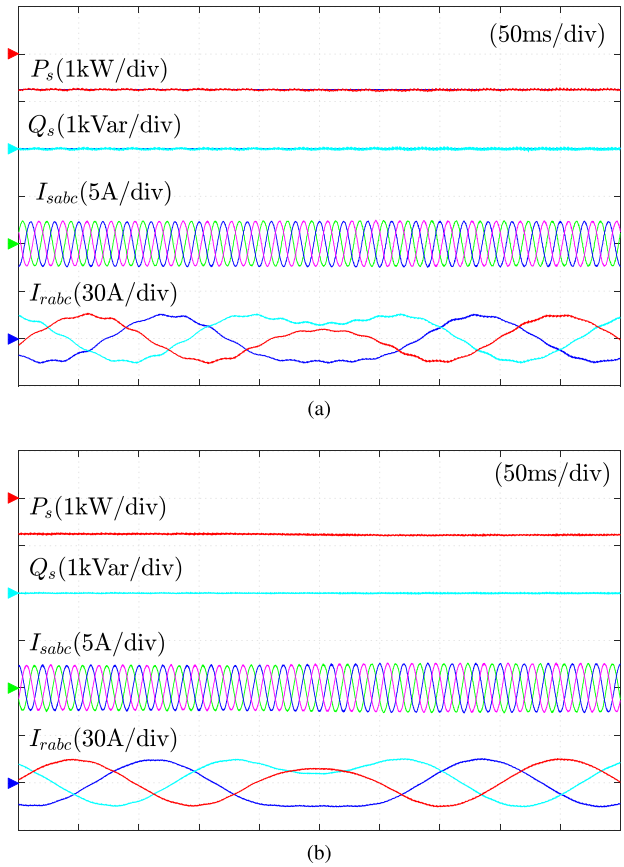

Fig. 6. Dynamic responses when the rotor speed changes from subsynchronous speed to supersynchronous speed. (a) MFPCC based on differential algebra. (b) MFPCC based on ESO.

mutual inductance. In Fig. 7(b), because the mutual inductance parameter is used in the calculation of the rotor current reference value in ADRC [10], [11], its reactive power and current will also change when the mutual inductance parameter differs from its actual value. However, in Fig. 7(c), regardless of whether the inductance parameter changes, the control performance of the proposed method is constant and good, exhibiting strong parameter robustness.

Although this article considers only a change in the inductance parameters, according to the analysis in Section II, the influence of the change in the inductance parameter is the greatest; thus, the effectiveness of the proposed method will not be affected when other parameters are changed individually or simultaneously.

To further verify the parameter robustness of the proposed method, Fig. 8 shows the experimental results at steady state corresponding to different α values. In Fig. 8(a), when α increases, the current THD and power ripple become larger, but the system is still stable and under control. However, in Fig. 8(b), when α is reduced to -100, the control is hardly affected. Table II lists the stator and rotor current THDs corresponding to different α values. It can be seen that the proposed method presents low THD of stator and rotor currents ($<5\%$) in a wide range of α values, exhibiting strong robustness against the variation in α.

TABLE II
CURRENT THD CORRESPONDING TO DIFFERENT α VALUES

The value of α	The THD of $\boldsymbol{i}_{sa}$	The THD of $\boldsymbol{i}_{ra}$
$\alpha = -35$	15.5434%	11.8997%
$\alpha = -40$	3.8904%	4.3105%
$\alpha = -50$	1.6088%	3.3376%
$\alpha = -70$	1.8901%	2.5503%
$\alpha = -80$	2.1887%	2.2607%
$\alpha = -100$	2.3644%	1.8946%

B. *Responses Under Unbalanced and Distorted Grids*

This section uses the regenerative grid simulator in Fig. 3(a) to set up an unbalanced and distorted grid to verify the effectiveness of the proposed method. The phase A voltage dips to 70% of its nominal value, and the fifth and seventh harmonics are added to the three-phase voltage. The amplitudes of the fifth and seventh harmonics are 7% and 5% of the fundamental component, respectively.

From top to bottom, Fig. 9(a) presents the stator-side active power, reactive power, three-phase stator current, rotor current, and grid line voltage $\boldsymbol{u}_{ab}$ and $\boldsymbol{u}_{bc}$, where the dashed line indicates

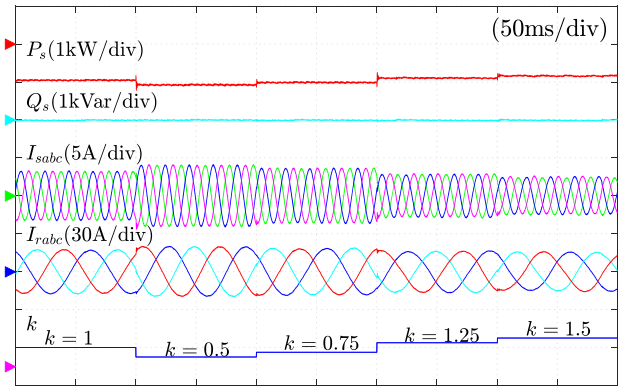

(a)

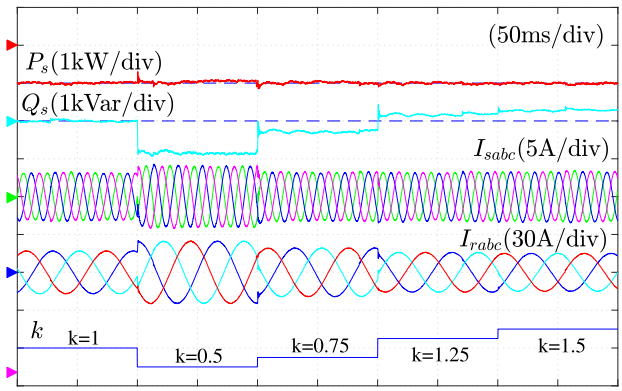

(b)

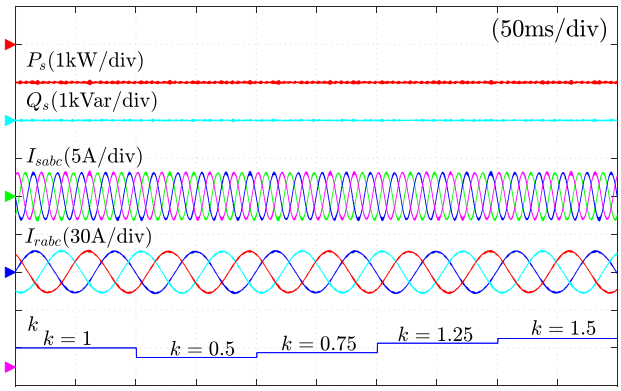

(c)

Fig. 7. Experimental results of three control methods when the mutual inductance changes. (a) Conventional DPC-SVM. (b) ADRC in [10] and [11]. (c) Proposed MFPCC based on ESO.

the corresponding reference value. Under an unbalanced and distorted grid, if the stator current reference is directly calculated according to (10), then the stator current will be unbalanced, and severe distortion will occur. In Fig. 9(b), the stator current reference is calculated according to (34), which means that the stator current reference contains only the positive fundamental components. As a result, it is clearly seen that the stator current does not contain obvious low-order harmonics and that the rotor current harmonics are also reduced to a certain extent. Fig. 10 shows the stator current THD of the two current reference

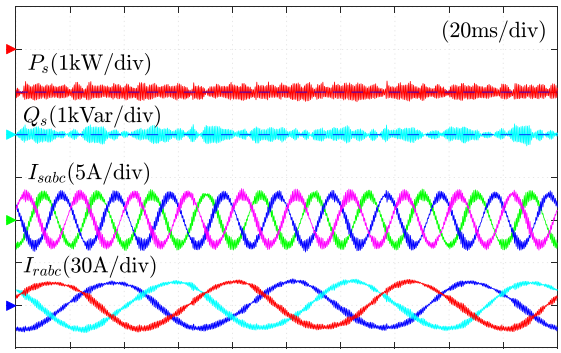

(a)

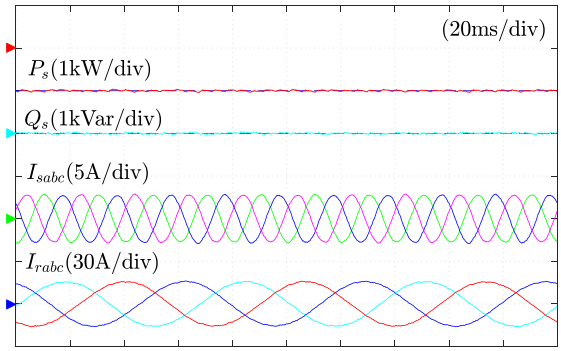

(b)

Fig. 8. Steady-state performance of the proposed MPFCC with different α values. (a) $\alpha = -35$. (b) $\alpha = -100$.

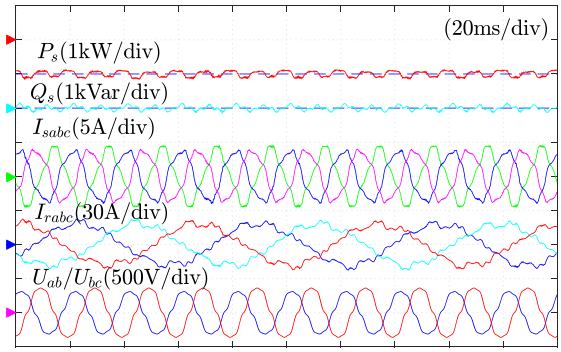

(a)

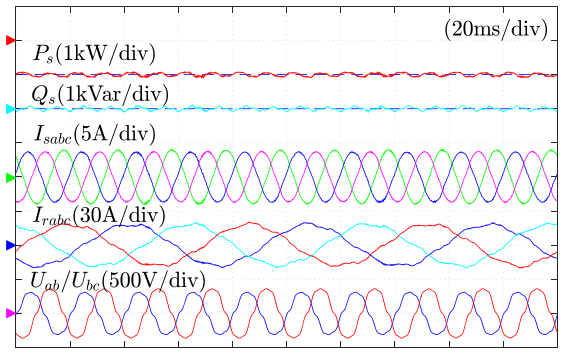

(b)

Fig. 9. Steady-state performances of the proposed MFPCC based on ESO under an unbalanced and distorted grid condition. (a) Conventional stator current reference calculation method. (b) Proposed stator current reference calculation method.

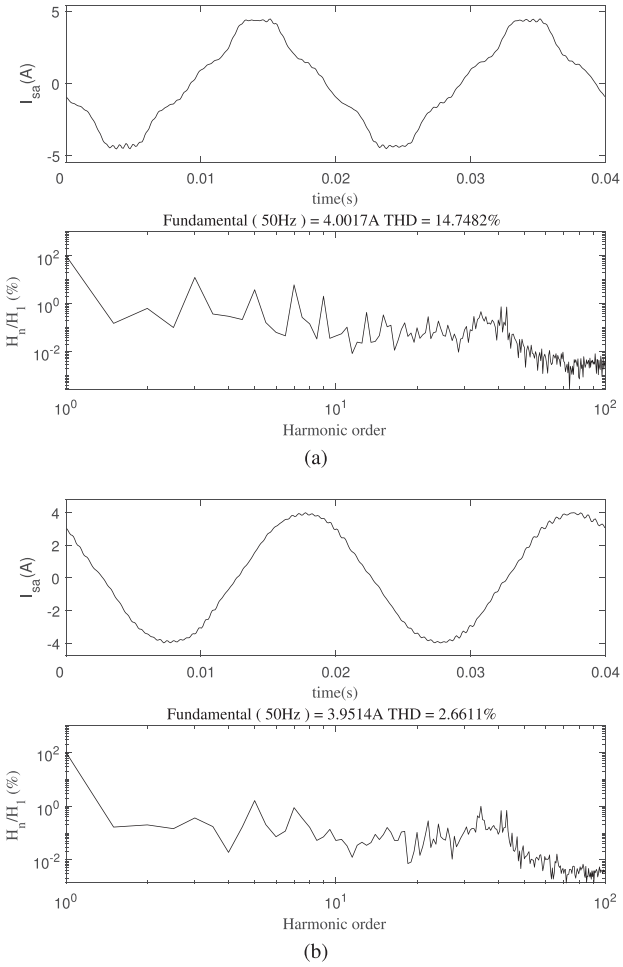

Fig. 10. Stator current THD of the proposed MFPCC based on an ESO under an unbalanced and distorted grid condition. (a) Conventional stator current reference calculation method. (b) Proposed stator current reference calculation method.

calculation methods. It is seen that the stator current THD is reduced from 14.75% to 2.66% when using the proposed stator current reference calculation method.

The actual grid frequency may deviate from its nominal value. Fig. 11 shows the experimental results of grid frequency changes. In Fig. 11(a), the grid frequency steps from 50 to 45 Hz at 0.25 s. In Fig. 11(b), the grid frequency steps from 50 to 55 Hz at 0.25 s. The proposed method uses grid frequency information in one-step delay compensation (11). For unbalanced and distorted grids, grid frequency fluctuations also affect the calculation of the stator current reference. In can be seen from Fig. 11(a) that a significant reduction in grid frequency has a great impact on the system. The rotor current no longer maintains sinusoidal symmetry, and there are significant stator current harmonics and power ripples. However, when the grid frequency suddenly increases sharply, the stator current and power are hardly affected except that the rotor current amplitude decreases, as shown in Fig. 11(b). To improve the performance under grid frequency changes, a frequency-locked loop may be added to observe the grid frequency online in the future.

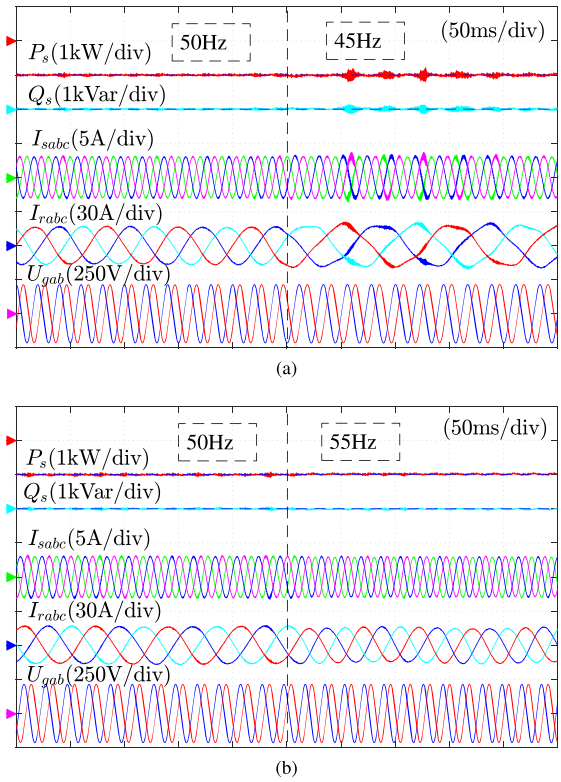

Fig. 11. Experimental results of the proposed MFPCC based on an ESO under grid frequency fluctuation. (a) Grid frequency decreasing from 50 to 45 Hz. (b) Grid frequency increasing from 50 to 55 Hz.

VI. Conclusion

To solve the problem of a poor control performance in response to parameter changes during the operation of a DFIG, this article combines an ultralocal model with PCC and uses an ESO to estimate the system disturbance to further improve the control performance. The final control expression obtained by the proposed method includes only reference values and measured values and does not contain any motor parameters. In addition, the proposed method is easy to implement, and only one parameter of the ESO needs to be designed. The proposed method is compared to the conventional DPC-SVM and ADRC. Experiments verify that the proposed method has quite good steady state and dynamic control performance regardless of whether the parameters change. In addition, under unbalanced and distorted grids, by calculating the stator current reference from the positive sequence component of stator voltage, sinusoidal and balanced three-phase stator currents can be obtained without changing the inner control loop.

References

[1] X. Wei, M. Cheng, J. Zhu, H. Yang, and R. Luo, "Finite-set model predictive power control of brushless doubly fed twin stator induction generator," *IEEE Trans. Power Electron.*, vol. 34, no. 3, pp. 2300–2311, Mar. 2019.

[2] R. Pena, J. C. Clare, and G. M. Asher, "Doubly fed induction generator using back-to-back PWM converters and its application to variable-speed wind-energy generation," *IEE Proc.—Elect. Power Appl.*, vol. 143, no. 3, pp. 231–241, May 1996.

[3] L. Xu and P. Cartwright, "Direct active and reactive power control of DFIG for wind energy generation," *IEEE Trans. Energy Convers.*, vol. 21, no. 3, pp. 750–758, Sep. 2006.
[4] A. Ejlali and D. A. Khaburi, "Power quality improvement using nonlinear-load compensation capability of variable speed DFIG based on DPC-SVM method," in *Proc. 5th Annu. Int. Power Electron., Drive Syst. Technol. Conf.*, Feb. 2014, pp. 280–284.
[5] Y. Zhang, J. Jiao, D. Xu, D. Jiang, Z. Wang, and C. Tong, "Model predictive direct power control of doubly fed induction generators under balanced and unbalanced network conditions," *IEEE Trans. Ind. Appl.*, vol. 56, no. 1, pp. 771–786, Jan./Feb. 2020.
[6] R. Bhattarai, N. Gurung, S. Ghosh, and S. Kamalasadan, "Parametrically robust dynamic speed estimation based control for doubly fed induction generator," *IEEE Trans. Ind. Appl.*, vol. 54, no. 6, pp. 6529–6542, Nov. 2018.
[7] R. Errouissi, A. Al-Durra, S. M. Muyeen, S. Leng, and F. Blaabjerg, "Offset-free direct power control of DFIG under continuous-time model predictive control," *IEEE Trans. Power Electron.*, vol. 32, no. 3, pp. 2265–2277, Mar. 2017.
[8] C. He, J. Hu, and X. Ran, "Finite control set model predictive current control for PMSM based on extended state observer," in *Proc. 14th IEEE Conf. Ind. Electron. Appl.*, Jun. 2019, pp. 804–809.
[9] L. Guo, D. Wang, L. Diao, and Z. Peng, "Direct voltage control of stand-alone DFIG under asymmetric loads based on non-singular terminal sliding mode control and improved extended state observer," *IET Elect. Power Appl.*, vol. 13, no. 7, pp. 958–968, 2019.
[10] A. Boukhriss, A. Essadki, A. Bouallouch, and T. Nasser, "Maximization of generated power from wind energy conversion systems using a doubly fed induction generator with active disturbance rejection control," in *Proc. 2nd World Conf. Complex Syst.*, Nov. 2014, pp. 330–335.
[11] H. Laghridat, A. Essadkil, M. Annoukoubil, and T. Nasser, "Linear active disturbance rejection control (LADRC) of a variable speed wind energy conversion system using a DFI-generator," in *Proc. 6th Int. Renewable Sustain. Energy Conf.*, Dec. 2018, pp. 1–6.
[12] C. Lin, T. Liu, J. Yu, L. Fu, and C. Hsiao, "Model-free predictive current control for interior permanent-magnet synchronous motor drives based on current difference detection technique," *IEEE Trans. Ind. Electron.*, vol. 61, no. 2, pp. 667–681, Feb. 2014.
[13] M. Fliess and C. Join, "Model-free control and intelligent PID controllers: Towards a possible trivialization of nonlinear control," *IFAC Proc. Vol.*, vol. 42, no. 10, pp. 1531–1500, 2009.
[14] Y. Zhou, H. Li, R. Liu, and J. Mao, "Continuous voltage vector model-free predictive current control of surface mounted permanent magnet synchronous motor," *IEEE Trans. Energy Convers.*, vol. 34, no. 2, pp. 899–908, Jun. 2019.
[15] Y. Song and H. Nian, "Sinusoidal output current implementation of DFIG using repetitive control under a generalized harmonic power grid with frequency deviation," *IEEE Trans. Power Electron.*, vol. 30, no. 12, pp. 6751–6762, Dec. 2015.
[16] P. Xiong and D. Sun, "Backstepping-based DPC strategy of a wind turbine-driven DFIG under normal and harmonic grid voltage," *IEEE Trans. Power Electron.*, vol. 31, no. 6, pp. 4216–4225, Jun. 2016.
[17] Y. Zhang, J. Jiao, and D. Xu, "Direct power control of doubly fed induction generator using extended power theory under unbalanced network," *IEEE Trans. Power Electron.*, vol. 34, no. 12, pp. 12024–12037, Dec. 2019.
[18] M. I. Martinez, A. Susperregui, G. Tapia, and L. Xu, "Sliding-mode control of a wind turbine-driven double-fed induction generator under non-ideal grid voltages," *IET Renewable Power Gener.*, vol. 7, no. 4, pp. 370–379, Jul. 2013.
[19] D. Sun, X. Wang, H. Nian, and Z. Q. Zhu, "A sliding-mode direct power control strategy for DFIG under both balanced and unbalanced grid conditions using extended active power," *IEEE Trans. Power Electron.*, vol. 33, no. 2, pp. 1313–1322, Feb. 2018.
[20] Y. Wang, Q. Wu, W. Gong, and M. P. S. Gryning, "H_∞ robust current control for DFIG-based wind turbine subject to grid voltage distortions," *IEEE Trans. Sustain. Energy*, vol. 8, no. 2, pp. 816–825, Apr. 2017.
[21] Y. Zhang, J. Hu, and J. Zhu, "Three-vectors-based predictive direct power control of the doubly fed induction generator for wind energy applications," *IEEE Trans. Power Electron.*, vol. 29, no. 7, pp. 3485–3500, Jul. 2014.
[22] L. Michel, C. Join, M. Fliess, P. Sicard, and A. Chériti, "Model-free control of dc/dc converters," in *Proc. IEEE 12th Workshop Control Modeling Power Electron.*, Jun. 2010, pp. 1–8.
[23] M. Mboup, C. Join, and M. Fliess, "Numerical differentiation with annihilators in noisy environment," *Numer. Algorithms*, vol. 50, no. 4, pp. 439–467, 2009.
[24] M. Fliess and C. Join, "Model-free control," *Int. J. Control*, vol. 86, no. 12, pp. 2228–2252, 2013.
[25] J. Han, "From PID to active disturbance rejection control," *IEEE Trans. Ind. Electron.*, vol. 56, no. 3, pp. 900–906, Mar. 2009.
[26] Z. Gao, "Scaling and bandwidth-parameterization based controller tuning," in *Proc. Amer. Control Conf.*, vol. 6, Jun. 2003, pp. 4989–4996.
[27] Z. Song, C. Xia, and T. Liu, "Predictive current control of three-phase grid-connected converters with constant switching frequency for wind energy systems," *IEEE Trans. Ind. Electron.*, vol. 60, no. 6, pp. 2451–2464, Jun. 2013.
[28] Q. Xu, M. Sun, Z. Chen, and D. Zhang, "Analysis and design of the extended state observer using internal mode control," in *Proc. 32nd Chin. Control Conf.*, Jul. 2013, pp. 5408–5413.
[29] L. Li, H. Nian, L. Ding, and B. Zhou, "Direct power control of DFIG system without phase-locked loop under unbalanced and harmonically distorted voltage," *IEEE Trans. Energy Convers.*, vol. 33, no. 1, pp. 395–405, Mar. 2018.
[30] Y. F. Wang and Y. W. Li, "Three-phase cascaded delayed signal cancellation PLL for fast selective harmonic detection," *IEEE Trans. Ind. Electron.*, vol. 60, no. 4, pp. 1452–1463, Apr. 2013.

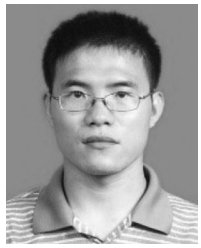

Yongchang Zhang (Senior Member, IEEE) received the B.S. degree from Chongqing University, Chongqing, China, in 2004 and the Ph.D. degree from Tsinghua University, Beijing, China, in 2009, both in electrical engineering.

From 2009 to 2011, he was a Postdoctoral Fellow with the University of Technology Sydney, Sydney, Australia. He joined North China University of Technology, as an Associate Professor in August 2011. He is currently a Full Professor and the Director of Inverter Technologies Engineering Research Center of Beijing, Beijing. He has published more than 100 technical papers in the area of motor drives, pulsewidth modulation, and ac/dc converters. His current research interest include model predictive control for power converters and motor drives.

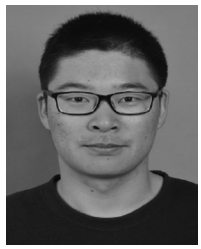

Tao Jiang was born in 1995. He received the B.S. degree in electrical engineering in 2017 from North China University of Technology, Beijing, China, where he is currently working toward the M.S. degree in control science and engineering.

His research interests include predictive control of doubly fed induction generators and brushless doubly fed machine.

Jian Jiao was born in 1993. He received the B.S. degree in electrical engineering from Shijiazhuang Tiedao University, Hebei, China, in 2015, and the M.S. degree in electrical engineering from North China University of Technology, Beijing, China, in 2019. He is currently working toward the Ph.D. degree with Beijing Jiaotong University, Beijing.